CHAPTER II: PLANET MARS – THE BACKGROUND

Like Earth, its neighbour planet, Mars, is a terrestrial planet with a solid surface, an atmosphere, two ice-covered pole caps, and not one but two moons (Phobos and Deimos). Some differences, such as a greater distance to the sun, a smaller diameter, a thinner atmosphere, and the longer duration of a year distinguish Mars from the Earth, not to forget the absence of life…so far.

Nevertheless, there are many correlations between terrestrial and Martian geological and geomorphological processes, permitting researchers to apply knowledge from terrestrial studies more or less directly to Mars. However, a closer look reveals that the dissimilarities, though few, can make fundamental differences in process background and development. The following chapter provides a brief but necessary insight into the geological and physical background of this planet, imparting to the reader some fundamental knowledge about Mars, which is useful for understanding this work.

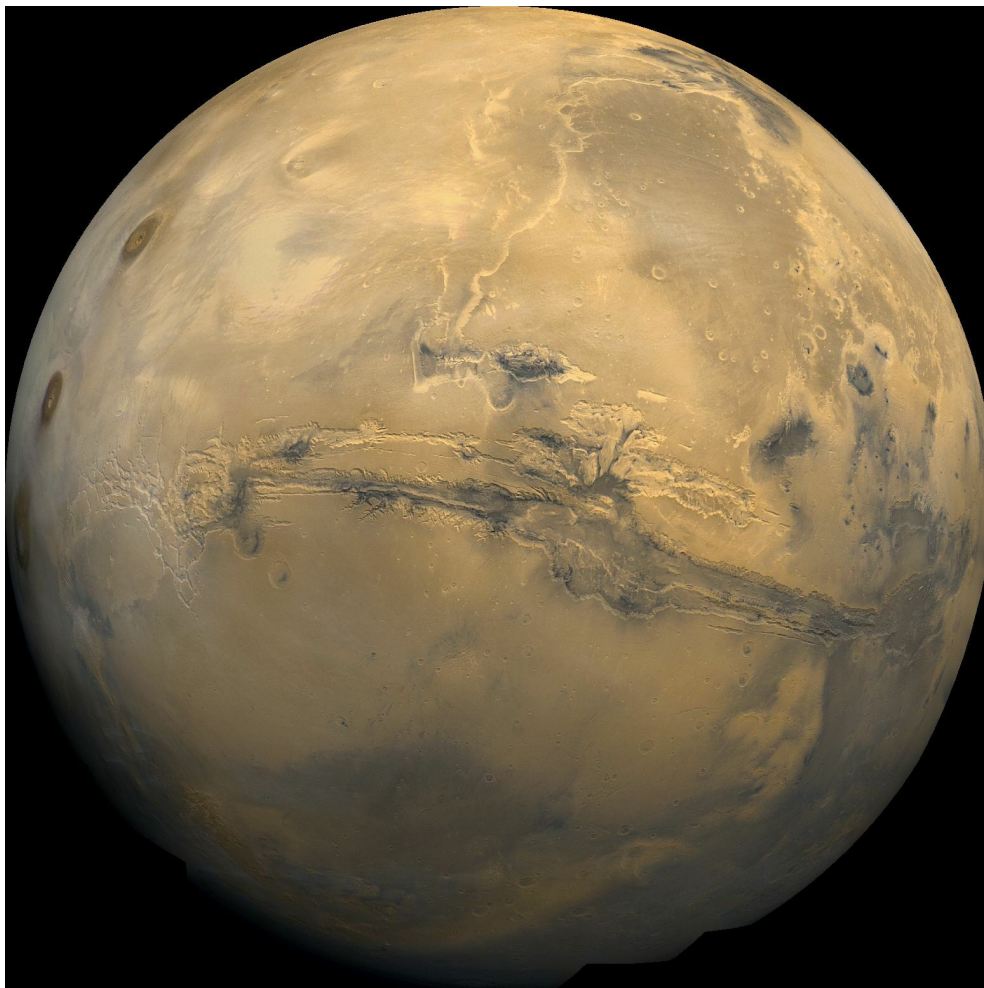Fig. 1 presents an impression of Mars viewed from space.

Figure 1: The planet Mars: a global view (Viking 1 Orbiter mosaic [NASA]).

Table 1 provides a summary of some major astronomical and physical parameters of Mars, giving the reader an impression of the extent to which they differ from terrestrial values.

Table 1: Parameters of Mars [*Kieffer et al.*, 1992a].

Property	Dimension
Orbit	227 940 000 km (1.52 AU) mean distance to the Sun
Diameter	6794 km
Mass	$6.4185 * 10^{23}$ kg
Mean density	~3.933 g/cm^3
Obliquity relative to orbital plane	25.19°
Inclination	1.85°
Duration of a Martian day (SOL)	24 h 37 min and 22 sec
Duration of a year in Martian days	669 Martian solar days (equals 687 Earth days)
Average temperature	210K (-63° C)
Lowest temperature	140K (-133° C) (at the polar caps on the winter side)
Highest temperature	300K (+27° C) (during the day on the summer side)
Surface area	144×10^6 km^2, approximately the same as the Earth
Atmospheric pressure at surface	6.5 mbar, less than 1 % compared to the atmospheric pressure on Earth
Composition of the atmosphere (Vol%)	95.32 % Carbon dioxide, 2.7 % Nitrogen, 1.6 % Argon, 0.13 % Oxygen
Moons	Phobos - diameter 22 km, orbit 5981 km above the surface Deimos - diameter 12 km, orbit 20,062 km above the surface

2.1 Martian Geology and Topography

Martian geology has passed through three historical phases reflected in three distinct stratigraphic time periods on Mars, as revealed by topographical, geomorphological, and spectral properties of the surface. *Tanaka* (1986) specified the current time-stratigraphic system of geologic periods based on relative rock ages. The crater size-frequency distribution per area derived from cumulative crater counts [*Neukum*, 1983] was used to distinguish different surface ages. This dating method will be introduced in Sect. 2.1.2. The boundary conditions for the geologic periods were deduced from the frequency of craters with a diameter equal to or larger than 2 km, 5 km, and 16 km. The oldest period, called the Noachian, lasted until 3.6 Ga before present. Characterised by the greatest number of large impact craters, it was named after the heavily cratered, ancient terrain in Noachis Terra. Called the Hesperian, the following period extended from 3.6 to 3.1 Ga before present and was characterised by a smaller number of relatively big craters. It was

named after the ridged plains material in Hesperia Planum. The most recent geologic period is called the Amazonian. It began 3.1 Ga before present. Surfaces dated to this period exclusively feature relatively small impact craters and smooth plains, such as Arcadia Planum which is located in the Amazonis Quadrangle, the eponym for this period. These three periods are further subdivided into several epochs (see Table 2).

Table 2: Martian stratigraphic time-system of geological epochs.
Stratigraphy after *Tanaka* (1986), model ages after *Hartmann and Neukum* (2001). Hesperian and Amazonian ages are subdivided into ages based on Neukum (N) and Hartmann (H) data. (Table adapted from *Jaumann* (2003), modified)

Stratigraphic epoch	Age [Ga before present]
Late Amazonian	0.55(n) / 0.3(H) − present
Middle Amazonian	2.1(N) / 1.4(H) − 0.55(n) / 0.3(H)
Early Amazonian	3.1(N) / 2.9(H) − 2.1(N) / 1.4(H)
Late Hesperian	3.6 – 3.1(N) / 2.9(H)
Early Hesperian	3.7 – 3.6
Late Noachian	3.8 – 3.7
Middle Noachian	3.95 – 3.8
Early Noachian	4.65 – 3.95

Geologic maps based on this information were drawn up by *Scott and Tanaka* (1986), *Greeley and Guest* (1987), and *Tanaka and Scott* (1987). A comprehensive proposal for the designation of Martian provinces ('quadrangles') and the nomenclature of prominent topographic features was developed by a working group headed by the International Astronomical Union (IAU) and published by *de Vaucouleurs et al.* (1975). The topography of the Martian crust shows a clear dichotomy between the heavily cratered plains of the southern highlands and the smooth plains of the northern lowlands. Two huge impact basins called Hellas and Argyre intersect the highland rocks, whereas a third giant impact basin, Isidis Planum, is located at the highland-lowland boundary. Further distinct geological units include the volcanic provinces of Tharsis and Elysium and the highland paterae (see Sect. 2.1.1). The Tharsis bulge represents coevally the major tectonic region on Mars associated with the huge tectonic graben system Valles Marineris, named after the missions Mariner 9, and numerous faults and trenches called fossae and catenae. Detailed information about tectonic processes on Mars is given in *Banerdt et al.* (1992). At the Tharsis centre at the western end of Valles Marineris there is a unique system of complex intersecting valleys called the Noctis Labyrinthus. Eastwards, Valles Marineris is connected with a region of chaotic terrains, the origin of enormous outflow channels formerly draining into the northern plain of Chryse Planitia. Both polar regions exhibit permanent ice caps composed of water and carbon dioxide ice, which are influenced by seasonal variations in condensation and sublimation that cause the upper CO_2 ice layer at

the north pole to disappear [*Tanaka et al.*, 1992]. These ice caps are surrounded by sequences of thick layered deposits alternating between bright and dark called layered terrains, interpreted as a mixture of ice and dust. While the south polar region is characterised by cratered Noachian and Hesperian highland rocks, the north polar region is covered by younger late Amazonian aeolian deposits associated with dune fields (see Sect. 3.4) [*Tanaka et al.*, 1992; *Jaumann*, 2003].

Aeolian, volcanic, fluvial, and glacial processes formed the Martian surface to a variable extent and time (see following sections and e.g. *Carr* (1973), *Scott* (1982), *Greeley et al.*, (1992), *Malin et al.* (1998), *Edgett and Malin* (2000b), *Greeley et al.* (2001), *Head et al.*, (2001), *Masson et al.* (2001), *Jaumann et al.* (2002), and *Neukum et al.* (2007)). According to *Bandfield* (2000), the surface composition of Mars exhibits two major Surface Types, roughly aligned to the planetary dichotomy. Surface Type 1 governs the southern hemisphere and is dominated by plagioclase, clinopyroxene, and feldspar [*Bandfield*, 2000], pointing to a basaltic composition. This alkaline extrusive volcanic rock can also comprise olivine minerals and is likewise common on Earth [*Matthes*, 2001]. Surface Type 2, which dominates the northern hemisphere, is of andesitic composition and is characterised by plagioclase, feldspar, and volcanic glasses [*Bandfield*, 2000]. Today, the Martian surface is covered to a variable extent by mobile materials such as dust and sand [*Mustard*, 2002]. The following map presents an overview of the topographic features of Mars discussed above, indicating the distinct regions that will be referred to in the following chapters.
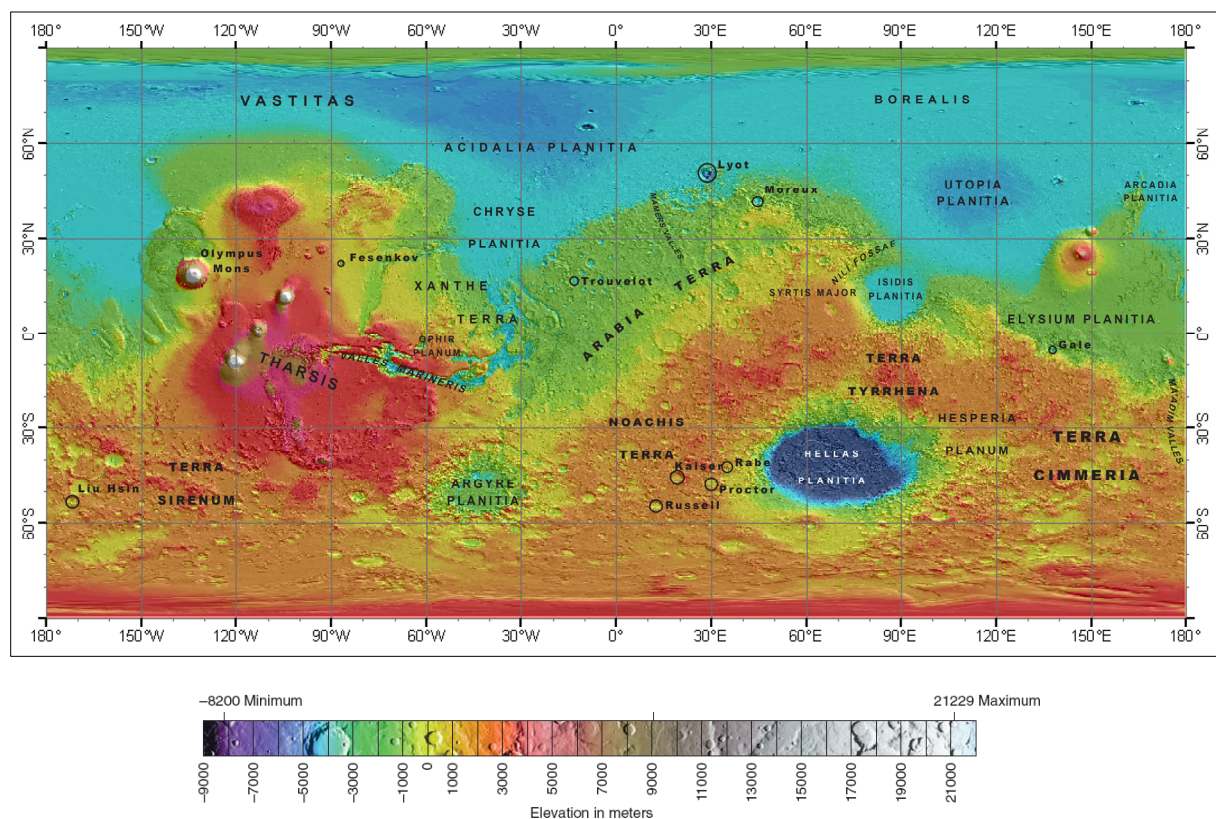

Figure 2: Topographic map of Mars (background: MOLA topography map).

2.1.1 Volcanism

Once a major surface-forming process on Mars, volcanism is responsible for a great variety of landforms such as shield volcanoes, tholi, paterae, small domes and cones, and vast volcanic plains [*Carr*, 1973; *Greeley and Spudis*, 1978; *Scott*, 1982; *Head et al.*, 2001; *Werner*, 2006], so that up to 60 % of the surface is covered with volcanic material [*Scott and Carr*, 1978]. Mars exhibits more than 35 labelled volcanoes concentrated in the volcanic provinces of Tharsis and Elysium as well as in the highland volcanic regions (Syrtis Major, Hesperia Planum, Malea Planum, and the Medusae fossae formation). The most prominent region is the Tharsis bulge with a height of up to 10km, comprising four huge basaltic shield volcanoes (Olympus Mons, Ascraeus Mons, Pavonis Mons, and Arsia Mons) with gentle slopes, complex coalescing calderas, and multiple lava flows and channels produced by effusive eruptions [*Carr*, 1974; *Scott*, 1982; *Jaumann*, 2003; *Werner*, 2006]. The highest mountain is Olympus Mons which, at about 22km, is the highest volcano in the solar system (Fig. 3).
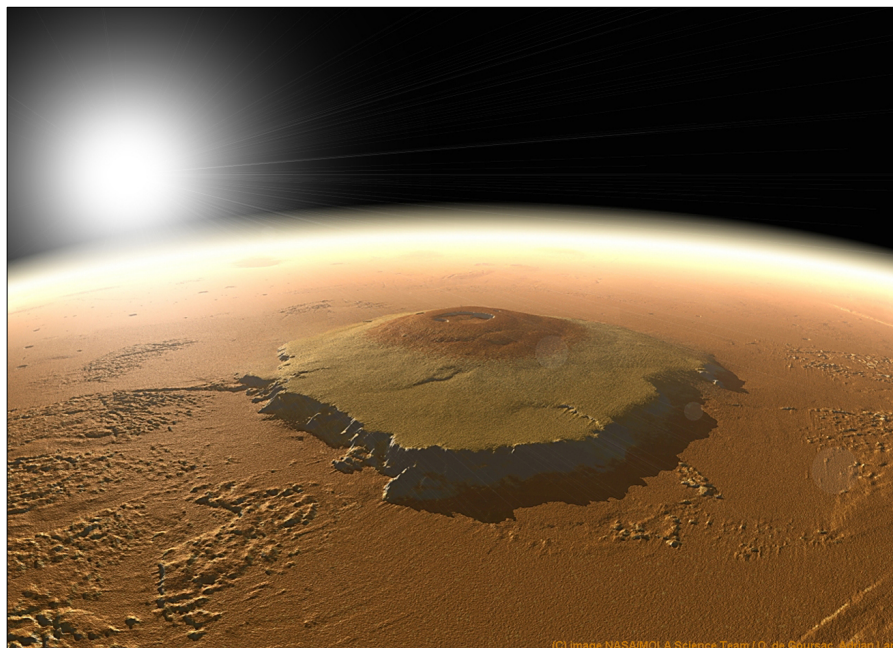

Figure 3: Artist's view of Olympus Mons (NASA/MOLA science team).

Volcanic activity on Mars started in the early Noachian, when widespread volcanism broke out in the highlands (see Table 3), followed in the Hesperian period by the onset of volcanism in Tharsis and Elysium as well as in Syrtis Major and the highland paterae. The late Amazonian is characterised by decreasing volcanic activity, beginning in Elysium province and later spreading to Tharsis. The most recent volcanic activity was dated to the last stages of the late Amazonian, characterised by decreasing activity in Elysium and the northern plains and the youngest Olympus Mons flows. This information is derived from dating volcanic features and landforms by assessing their crater size-frequency distribution. This pioneering method will be described in the next section.

2.1.2 Impact Cratering and Dating Method

Like other bodies with a solid surface but without a thick protecting atmosphere and efficient erosion processes, Mars is blotched by innumerable impact craters of various sizes and shapes. Crater diameters predominantly depend on impact energy, whereas the type and morphology of a crater may also be determined by the substrate (e.g. rampart craters with flow structures resembling ejecta blankets are thought to occur in water- or ice-bearing underground [*Carr et al.*, 1977]). Most of the Martian craters can be found in the ancient terrains of the southern highlands.

An age-dating technique for geological surfaces based on crater size-frequency distribution has been developed by *Neukum* (1983). The basic concept is that older surfaces exhibit a large number of huge impact craters, whereas younger surfaces are dominated by small impact craters. Large craters are few or lacking entirely because the abundance of big projectiles declined as the age of the universe increased. This revolutionary method was first developed for the Moon, where it could be calibrated absolutely by means of the radiometrically determined ages of Moon samples. The method was further developed and extrapolated to meet the conditions on Mars by *Hartmann & Neukum* (2001). The following figure shows the impact crater chronology curve for Mars in combination with related stratigraphic geologic periods.
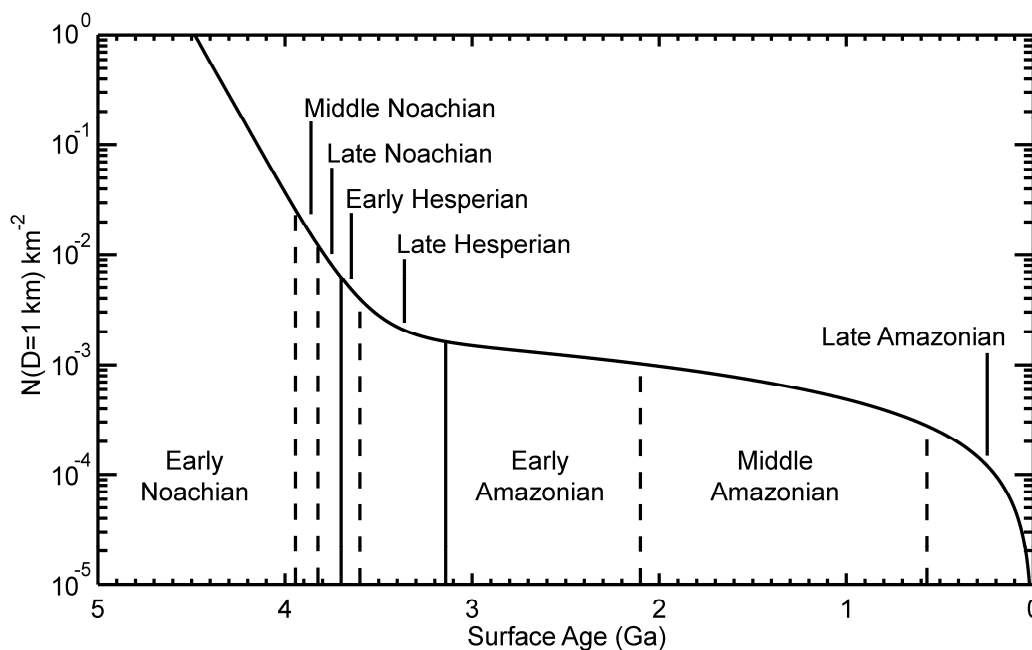

Figure 4: Martian impact cratering chronology curve by *Hartmann and Neukum* (2001) (graph adapted from *Werner* (2006)). The stratigraphy of chronological periods and epochs was defined by *Tanaka* (1986).

2.1.3 Erosion and Weathering

Erosion is possible on Mars because the presence of an atmosphere facilitates the interchange of volatiles between the surface and the atmosphere, leading to secondary modification of the surface materials and their morphology in association with weathering and material redistribution [*Jaumann,* 2003].

Erosional agents on Mars are wind, water, and ice. Furthermore, impact cratering and gravitative mass movements have left behind obvious morphological indications of their effect in the form of impact craters and landslides, for example. Erosional processes due to water, wind, ice, mass movements, and impact cratering and the associated morphological indications on Mars have been comprehensively discussed by *Jaumann* (2003). Due to the lack of significant amounts of liquid water, aeolian erosion, such as deflation and abrasion (also referred as to corrasion [*Leser*, 2003]), might be the dominant erosion process on Mars today. Deflation designates a process whereby loose particles, such as sand grains, are blown away. This removal of fine particles leaves behind coarser particles, resulting in deflation surfaces such as those at the Opportunity and Spirit landing sites on Mars [*Thomas et al.*, 2005]. Abrasion results from the impact of sand grains on solid rock or an indurated surface. The amount of abrasion depends on the kinetic energy of the grain, which is contingent on its mass and speed. The collision between the grain and the target may damage either one or both agents. Typical geomorphologic features produced by abrasion are ventifacts, which are flattened, polished surfaces often associated with facets, pits, flutes, and grooves [*Greeley and Iversen*, 1985; *Thomas et al.*, 2005].

Weathering processes are classified as either chemical or mechanical, depending on the influence of water. The action of most weathering processes, particularly the mechanical kind, depends on and is closely related to temperature changes, which cause weathering agents such as water molecules and salts to expand and contract. Salt weathering is supposed to be a significant weathering process on Mars, as comprehensively discussed by *Malin* (1974). One further dominant weathering mechanism on Mars might be thermal weathering (insolation weathering), given the absence of liquid water. Insolation raises the temperature of an originally compacted and thus solid substrate, resulting in material expansion, whereas a subsequent drop in temperature will cause material contraction. Repeated temperature changes, resulting in repeated expansion and contraction, will ultimately break up a formerly solid substrate. Material break-up caused by thermal weathering might be significant on Mars because diurnal temperature fluctuations are enormous, as measured at the Viking landing site where they reach 50°C [*Hauk et al.*, 2002].

A tabular overview of the time ranges and activities of geological and morphological processes on Mars is given in Table 3.

Table 3: Major events in the geological history of Mars (adapted from *Head et al.* (2001)). (Geological development and stratigraphy were derived from *Scott and Carr* (1978), *Greeley and Guest* (1987), *Tanaka and Scott* (1987), and *Geissler et al.* (1990a)).

	Volcanism	Tectonism	Fluvial events	Cratering	Erosion and surficial processes	No. of craters per 10^6 km^2
AMAZONIAN	• Late flows in southern Elysium Planitia. • Decreased volcanism in northern plains. • Most recent flows from Olympus Mons. • Emplacement of massive materials at south edge of Elysium Planitia. • Waning volcanism in Tharsis region. • Wanning volcanism in Elysium region. • Widespread flows around Elysium Mons.	• Tharsis tectonism continued through the Amazonian, mostly associated with the large shield volcanoes. • Formation of Elysium Fossae. • Initial formation of Olympus Mons aureoles.	• Channeling in southern Elysium Planitia. • Late period of channel formation. • Formation of channels NW of Elysium Mons.		• Emplacement of polar dunes and mantle. • Development of polar deposits? • Formation of ridged lobate deposits on large shield volcanoes. • Emplacement of massive materials at south edge of Elysium Planitia. • Local degradation and resurfacing of northern plains. • Erosion in northern plains. • Deep erosion of layered deposits in Valles Marineris. • Development of ridges, grooves, and knobs on northern plains.	>2 km 20 30 40 50 60 70 80 90 100 200 300 400 >5 km 50
HESPERIAN	• Volcanism at Syrtis Major. • Formation of highland paterae. • Volcanism at TempeTerra. • Major volcanism in Elysium and Tharsis regions. • Emplacement of ridged plains (Hr).	• Formation of Noctis Labyrinthus. • Formation of Valles Marineris. • Formation of wrinkle ridge systems. • Memnonia and Sirenum Fossae, fractures around Isidis.	• Development of large outflow channels. • Infilling of northern plains.		• Degradation of northern plains materials. • Dorsa Argentea formation at South Pole. • Resurfacing of northern plains.	60 70 80 90 100 500 600 700 800 900 1000 200
NOACHIAN	• Formation of intercrater plains. • Decreasing highland volcanism • Beginning of widespread highland volcanism.	• Ceraunius, Tempe, and Noctis Fossae. • Tectonism south of Hellas. • Archeron Fossae. • Claritas Fossae.	• Formation of extensive valley networks.	• Waning impact flux. • Intense bombardment. • Argyre impact. • Hellas and Isidis impacts. • Formation of oldest exposed rocks.	• Extensive desiccation and etching of highland rocks. • Formation and erosion of heavily cratered plateau surface. • Deep erosion of basement rocks.	300 400 500 600 >16 km 100 200 300 400

2.2 Martian Climate

The following section gives a brief overview of the basics of the Martian climate as far as they are relevant for this study. A more extensive introduction is available in *Reiss* (2006). A detailed examination is presented in *Kieffer et al.* (1992b).

2.2.1 Atmosphere

As Table 1 shows, the pressure of the Martian atmosphere amounts to no more than 0.75% of Earth's, the average being about 5.6 mbar. It is mainly composed of carbon dioxide (95.3%), nitrogen (2.7%), and argon (1.6%) [*Owen et al.*, 1977, *Kiefer et al.*, 1992]. The fraction of atmospheric water represents only 0.03%. Although oxygen is present in the Martian atmosphere, it accounts for no more than 0.13%. Due to the seasonal variation in CO_2 and H_2O condensation at the polar caps, all proportions vary seasonally. *Kiefer et al.* (1992) put this variation at up to 30%. Another reason why Martian surface pressure varies significantly is that elevations fluctuate by 13km (pressure varies significantly with elevation, from the deepest point at Hellas (7 torr at -8220 m) to the highest point at the summit of Olympus Mons (1 torr at 21229 m) [*Presley and Christensen*, 1997b]).

The evolution of an atmosphere, which is thought to have been much denser at some time in history, is attributed to intense outgassing processes caused by volcanism and impact bombardment [*Pollack et al.*, 1987]. For example, substantive indications of significant amounts of liquid water provide evidence that the physical requirements for stable liquid water (i.e. higher atmospheric pressure and density, but also higher average temperatures) must have existed on Mars for a long time. There are many morphological and mineralogical indications that the Martian climate has been much wetter and warmer in former times, followed by a dramatic climate change probably at the end of the Noachian [*Masson et al.*, 2001; *Jaumann et al.*, 2002; *Bibring et al.*, 2006]. Mars seems to have experienced a number of periodic climate fluctuations, probably caused by periodic oscillations in eccentricity and obliquity and/or by changes in the atmospheric dust content or the intensity of solar radiation [*Pollack*, 1979]. A comprehensive examination of the evolution, composition, and history of the Martian atmosphere is to be found in *Owen et al.* (1977), *Pollack* (1979), and *Owen* (1992).

2.2.2 Wind

Dominating the climate of Mars, wind is the major morphological forming process today, especially with regard to the transport of small particles like those discussed in this study. The frequent occurrence of vast dust storms [e.g. *James and Evans*, 1981; *Ryan and Sharman*, 1981; *Moore*, 1985; *Cantor et al.*, 2001] and small dust devils [e.g. *Cantor et al.*,

2006; *Stanzel et al.*, 2006] is an obvious sign of wind motion on Mars. A detailed introduction to the physics of wind conditions and wind speeds on Mars is given in Chapter III. At this point, only general aspects will be highlighted.

Due to the lack of oceans, the Martian surface responds quickly to solar heating, resulting in a less complicated circulation than on Earth. On the other hand, the greater topography has a strong effect, complicating the circulation pattern on Mars. Global circulation is determined by seasonal temperature gradients driven by summer-time heating on the summer hemisphere where warm air rises, descending again on the cooling winter hemisphere [*Cattermole*, 2001]. These variations are so immense that Mars exhibits the most dramatic seasonal changes in global atmospheric circulation yet observed on any planetary body in the solar system [*Magalhães*, 1987].

Modelling the Martian climate and weather, including predictions of circulation patterns and wind speeds, has a long history. Early studies were done, for example, by *Leovy and Mintz* (1969) and *Pollack et al.* (1976). Recently, climate models were developed and published by, among others, *Forget et al.* (1999), *Lewis et al.* (1999), and *Justus et al.* (2002), providing useful information for morphological studies. Fig. 5 shows such an exemplary global wind field for Mars derived from the Mars climate database (see also Sect. 4.7.1).
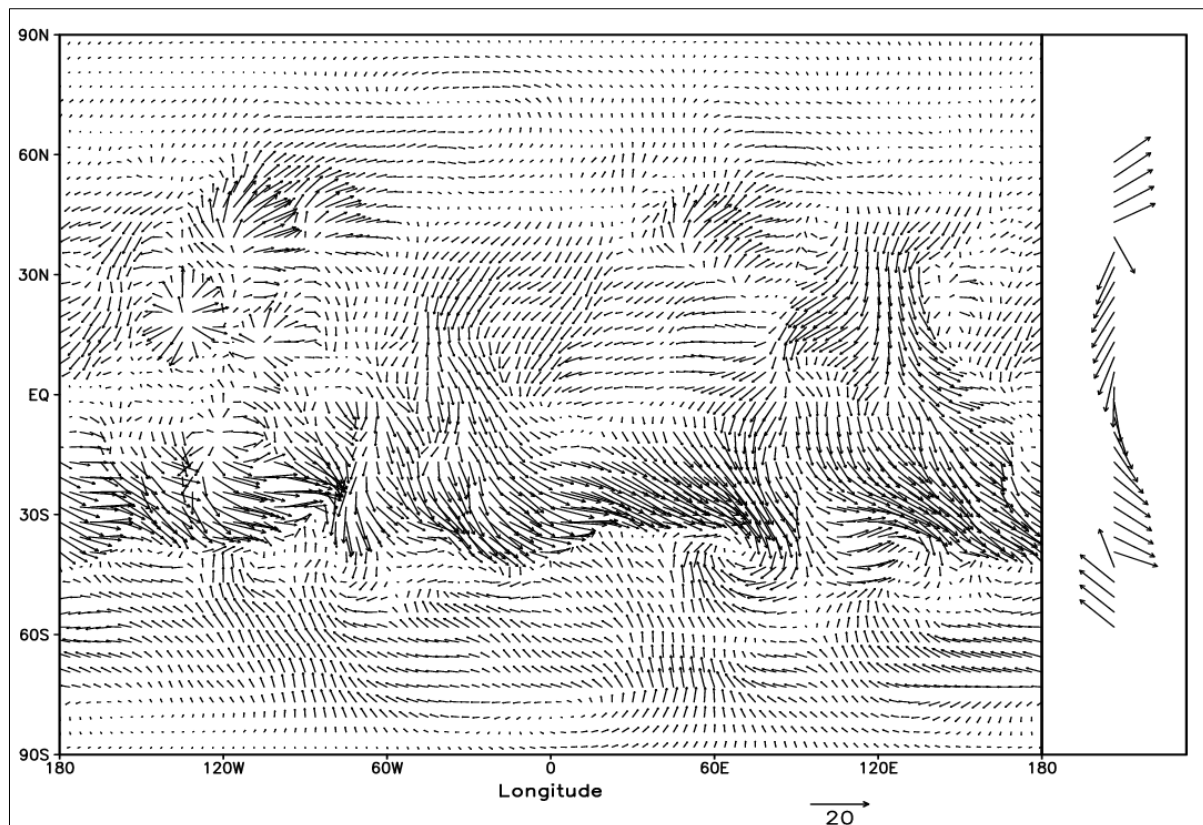

Figure 5: Global averaged wind field for Mars derived from the Mars Climate Database (MCD) [*Lewis et al.*, 1999]. The length of a vector correlates with the wind speed; a 20 m/s vector is shown for comparison. The right panel shows the zonal-mean wind direction between 60°S and 60°N.

2.2.3 Water

Although the current atmosphere does not provide the conditions for stable liquid water on Mars, the planet exhibits significant amounts of water in the form of ice, mainly stored in the polar caps. Moreover, the Martian atmosphere contains some water, as measured by water vapour column abundance. If all Martian atmospheric water were precipitated on the surface, the liquid water column would have a thickness of 10 μm [*Jakosky and Harberle*, 1992]. Vapour and ice are the only two stable aggregate states for water on Mars.

The existence of water on Mars was proven by spectrometer analyses, which showed typical absorption bands at specific wavelength positions. The Mars Atmospheric Water Detector (MAWD) on board the Viking orbiter delivered the first suggestions of the presence of water in the Martian atmosphere [e.g. *Jakosky and Farmer*, 1982]. Moreover, seasonal variations in the water vapour content of the north polar atmosphere supported the conclusion that water ice exists at the north polar cap [*Jakosky and Harberle*, 1992]. Atmospheric water frequently freezes to seasonal frost on surfaces in higher latitudes, and dune sands provide ideal conditions for the development of surface frost [e.g. *Malin and Edgett*, 2000; *Reiss and Jaumann*, 2002; *Schorghofer and Edgett*, 2006; *Di Achille et al.*, 2008]. Water ice has had a significant influence on Martian morphology. Evidence of earlier and recent glacial and periglacial processes includes relict debris covered glaciers, glacial troughs, or polygonal crack patterns [e.g. *Hauber et al.*, 2005; *van Gasselt*, 2007; *Di Achille and Ori*, 2008]. Morphological evidence of the former existence of huge amounts of liquid water over a relatively long time can be found in the Martian landscape at innumerable places, including valley networks, outflow channels, and former lakes associated with fluvial fan deltas [e.g. *Marchenko et al.*, 1998; *Baker*, 2001; *Masson et al.*, 2001; *Jaumann*, 2003; *Lanz*, 2004; *Di Achille et al.*, 2006; *Pondrelli et al.*, 2008]. Furthermore, hydrated minerals found in several regions on Mars [e.g. *Poulet et al.*, 2004; *Gendrin*, 2005; *Poulet et al.*, 2005; *Hauber et al.*, 2006; *Roach et al.*, 2007] and haematite marbles found at Meridiani Planum [e.g. *Catling*, 2004; *Squyres et al.*, 2006b; *Christensen et al.*, 2004b] document the former existence of water by the abundance of physically or chemically absorbed water molecules in their crystal lattices (see Sect. 5.3).

CHAPTER III: AEOLIAN PROCESSES ON MARS

Ralph A. Bagnold, who is considered to be the pioneer of the study of aeolian processes, first described the basic principles of aeolian transport in detail [*Bagnold*, 1954]. *Greeley and Iversen* (1985) and *Pye and Tsoar* (1990) updated and reviewed the subject, with the former additionally addressing the conditions on Mars.

Greeley et al. (1982) defined two principal requirements for aeolian processes to occur: first, presence of loose particles, and second, winds of sufficient strength to move them. The basic physics of windblown sand on Mars differs from that on Earth because of the different geophysical and atmospheric conditions. Elementary differences include lower atmospheric pressure and density as well as lower gravitational effects. The following chapter will introduce the theoretical background of aeolian grain movements on Mars and explain the conditions for the buildup of dunes and the underlying processes. Furthermore, it will provide a survey of aeolian bed forms on Mars and Earth.

3.1 The Physics of Particle Motion

Based on wind tunnel studies and field observations, *Bagnold* (1954) characterised three modes of particle movement by wind, depending on particle size and wind velocity: suspension (very small particles, mostly silt and clay), saltation (mostly sand grain-sized particles) and creep or surface traction (particles rolling, sliding and pushing along the surface [e.g. *Bagnold*, 1954; *Greeley and Iversen*, 1985; *Pye and Tsoar*, 1990; *Greeley et al.*, 2001].

The points of transition between these three modes of transport depend on *terminal speed* (u_f) and *threshold friction speed* (u_{*t}). The forces controlling a spherical particle falling through the air are aerodynamic drag, which keeps the particle aloft, and the particle's weight, which pulls it downward [*Greeley and Iversen*, 1985; *Edgett and Christensen*, 1991]. The acceleration of a particle dropped from rest will progress until the drag force is equal to the particle's weight. At this point, the particle has reached its terminal speed or terminal fall velocity, which *Edgett and Christensen* (1991) give as

$$u_f = \left(\frac{4\rho_p g D_p}{3\rho_a C_d} \right)^{0.5}$$

(1)

where ρ_p is particle density, g is gravitational acceleration, D_p is the particle diameter, ρ_a is atmospheric density, and C_d is the drag-off coefficient, which is a function of the Reynolds number $u_f D_p/v$. This dimensionless number describes the ratio of inertial to viscous forces

in a fluid flow, where v is the kinematic viscosity of the air [*Greeley and Iversen*, 1985; *Edgett and Christensen*, 1991]. Considering a sand grain at rest on a flat bed of loose grains under wind flow conditions, the forces of aerodynamic drag (F_d acting horizontally in the direction of motion), aerodynamic lift (F_l acting vertically upwards), and the particle's weight (F_g acting opposite to the lift force) are associated with interparticle forces (F_{ip}). The latter include electrostatic cohesion between neighbouring grains as well as adhesive forces (particularly in the case of very fine grains) acting between grains and other surfaces [*Iversen et al.*, 1976b; *Pye and Tsoar*, 1990; *Edgett and Christensen*, 1991; *Greeley et al.*, 1992]. An illustration of these forces is presented in Fig. 6.
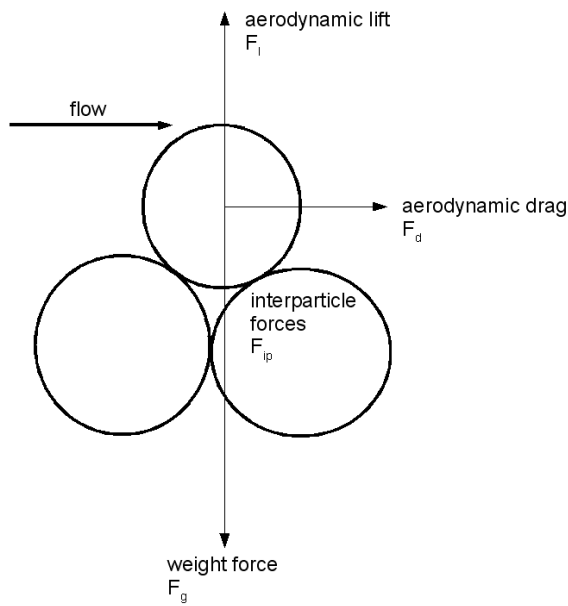
Figure 6: Sketch showing the primary forces acting on a spherical particle under aeolian conditions.

Consider now a slowly increasing wind velocity over a loose sandy surface. A sand grain will be lifted into the air when the aerodynamic lift force becomes paramount, i.e. when the terminal fall velocity of a particle is overcome by the upward current [*Bagnold*, 1954]. At this critical point the *surface friction speed* (u_*, or drag velocity) reaches its minimum value allowing particles to be raised by the lift force. This threshold velocity is called *threshold friction speed* (u_{*t}). It is a function of the *shear stress* τ (see Fig. 7) of the wind and depends on particle size and density (see Fig. 3), the density and viscosity of the atmosphere, and the acceleration of gravity on Mars [*Moore*, 1985]. The surface friction speed is directly proportional to the rate of wind-velocity increase with the log height above the surface [*Bagnold*, 1954; *Edgett and Christensen*, 1991]. It is equal to the square root of the ratio of shear stress (τ) to atmospheric density (ρ_a), given by

$$u_* = \sqrt{\frac{\tau}{\rho_a}} \qquad (2)$$

[*Bagnold*, 1954; *Pye and Tsoar*, 1990; *Edgett and Christensen*, 1991]

It must be noted that the surface friction speed is not a true wind velocity but a measure of the vertical component of the turbulent speed near the surface [*Greeley and Iversen*, 1985]. The mode of transport depends now on the proportion of the forces relative to each other. Upward sand grain transport by *suspension* begins when the terminal speed is lower than the friction speed ($u_f < u_*$). The trajectory of these fine particles can reach heights of several kilometres. Transport by *saltation* occurs when the terminal speed is much larger than the friction speed ($u_f >> u_*$). Under these conditions the trajectory of these mostly sand grain-sized particles is unaffected by turbulence, the path is lower and smoother and only reaches heights between a few centimetres and one meter [*Parteli*, 2001]. Transport by *creep* affects larger particles, which are too heavy to be transported by wind but can still be rolled or pushed along by the impact of grains due to the exchange of momentum. A detailed description of these processes is given in Fig. 7.
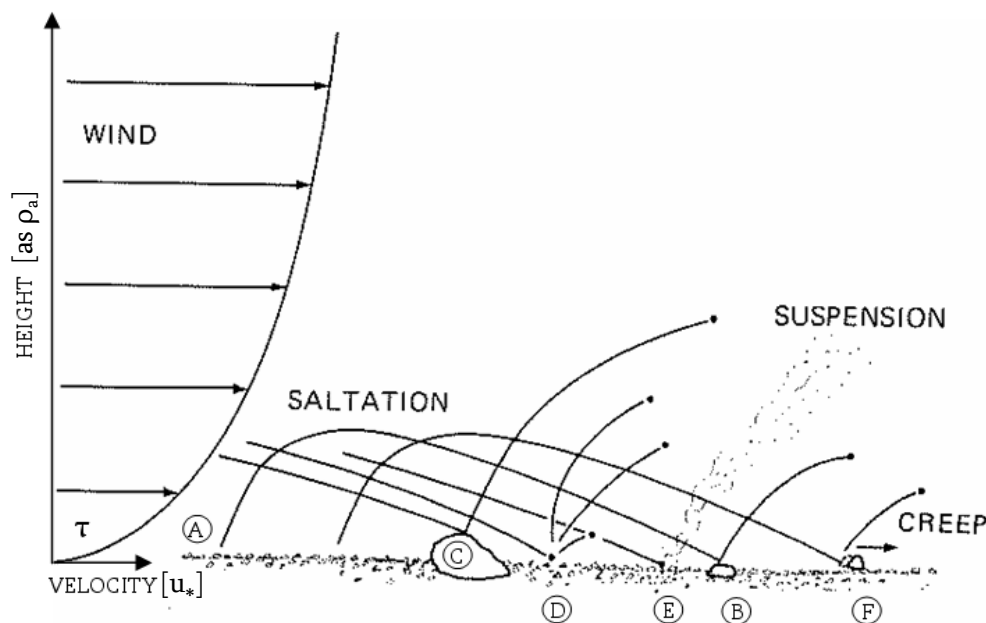

Figure 7: Diagram showing the three principal modes of aeolian grain transport (adapted from *Greeley & Iversen* (1985)).
On the left hand is a typical wind velocity profile above the surface through the boundary layer. Friction along the surface generates *shear stress* ($\tau = u_* \rho_a)^2$ which lifts particles into the atmosphere (A). The lifted particle is carried downwind back to the surface, from which it bounces (B) back into flight. This motion is called *saltation*. Particles hitting rocks, such as grains, (C) will elastically rebound into relatively high saltation trajectories. Furthermore, the rock at (C) might be eroded by the impact of the grain. The grain at (D) impinges on other grains at the surface, causing them to saltate. At point (E), a grain strikes some very fine particles at the surface which, due to cohesion, are too fine to be moved by wind alone at the assumed wind speed. These fine particles are dispersed in the atmosphere and carried in *suspension* by turbulences. At (F), a saltating grain strikes a larger grain at the surface and pushes it downwind for a short distance. This mode is called *creep* or *surface traction*. It was found that suspension and creep are often initiated or enhanced by saltation impact.
[*Greeley and Iversen*, 1985; *Greeley et al.*, 1992; *Greeley et al.*, 2001]

Bagnold (1954) observed in his wind tunnel experiments that the first movement of a grain before it passes into one of the other modes of transport is rolling. *Iversen et al.*

(1976b) predicted average threshold friction velocities for Mars as a function of particle size. They were followed by *Iversen and White* (1982), who estimated these threshold speeds for the conditions given on Earth, Mars, and Venus using different combinations of particle and gas densities. The results for Mars and Earth are shown in Fig. 8.
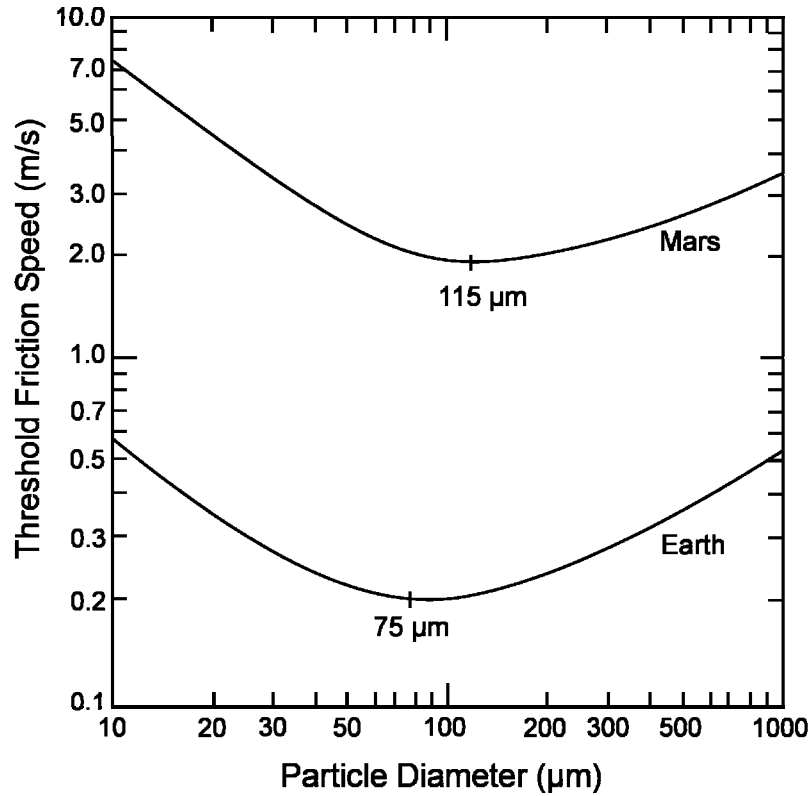

Figure 8: Average *threshold friction speeds* (u_{*t}) for Earth and Mars for particles of different sizes [*Edgett and Christensen* (1991); adapted from *Iversen and White* (1982)].

The discrepancies between Mars and Earth result from differences in atmospheric density and gravity. Particle density in either case is 2.65 g/cm³, Martian atmospheric density (ρ_M) is 1.10 x 10⁻⁵ g/cm³, terrestrial atmospheric density (ρ_E) is 1.23 x 10⁻³ g/cm³, Mars atmosphere kinematic viscosity (v_M) is 11.19 cm²/s, Earth atmosphere kinematic viscosity (v_E) is 0.146 cm²/s, Mars gravitational acceleration (g_M) is 375 cm/s², Earth gravitational acceleration (g_E) is 981 cm/s². The optimum particle sizes for saltation are indicated (75 µm for Earth and 115 µm for Mars).

Due to the lower atmospheric pressure and density on Mars, threshold friction velocities are 10 times higher than on Earth [*Greeley et al.*, 1980; *Edgett and Christensen*, 1991]. This means that higher wind speeds are required to move similar-sized grains on Mars than on Earth. Fig. 8 shows that the minimum threshold friction velocity needed to move grains of a size of 75 µm is about 0.2 m/s on Earth. On Mars, the minimum threshold friction velocity is about 2.2 m/s and the most easily moveable grain size is 115 µm. Based on the particle threshold curve in Fig. 9, *Greeley et al.* (1980) converted the friction velocity for sand grains of ~100 µm into an effective wind speed of 25-30 m/s under present Martian atmospheric conditions. Similar but slightly higher wind speeds were

calculated by *Sullivan et al.* (2005), who arrived at a wind speed *u* of ~45 m/s at 1m above the surface for a threshold friction velocity of 2.0 m/s. *Moore* (1985) reported on wind speeds of about 40 to 50 m/s at 1.6 m above the surface with corresponding friction speeds of 2.2-4.0 m/s during the Martian dust storm on Sol 1742, measured by the Viking Lander 1.

The cohesive effects of interparticle forces are responsible for the higher threshold velocities of smaller particles, whereas larger particles need higher friction velocities because of their greater weight (see Fig. 8 and 9) [*Iversen et al.*, 1976b; *Greeley et al.*, 1980; *Iversen and White*, 1982; *Edgett and Christensen*, 1991]. Note the influence of surface roughness on friction speed and the resultant effective wind speeds displayed as scale bars for different surface types in Fig. 9. The higher the surface roughness, the weaker the winds required to reach the friction speed needed for particle motion. Note also that temperature and air pressure affect the friction at the surface. The diagram shows the required friction speeds for four different air pressure values and various temperatures in order to account for this influence. For example, at a pressure of 5 mb at 150 K, a lower wind speed is required than at a higher temperature at the same pressure.
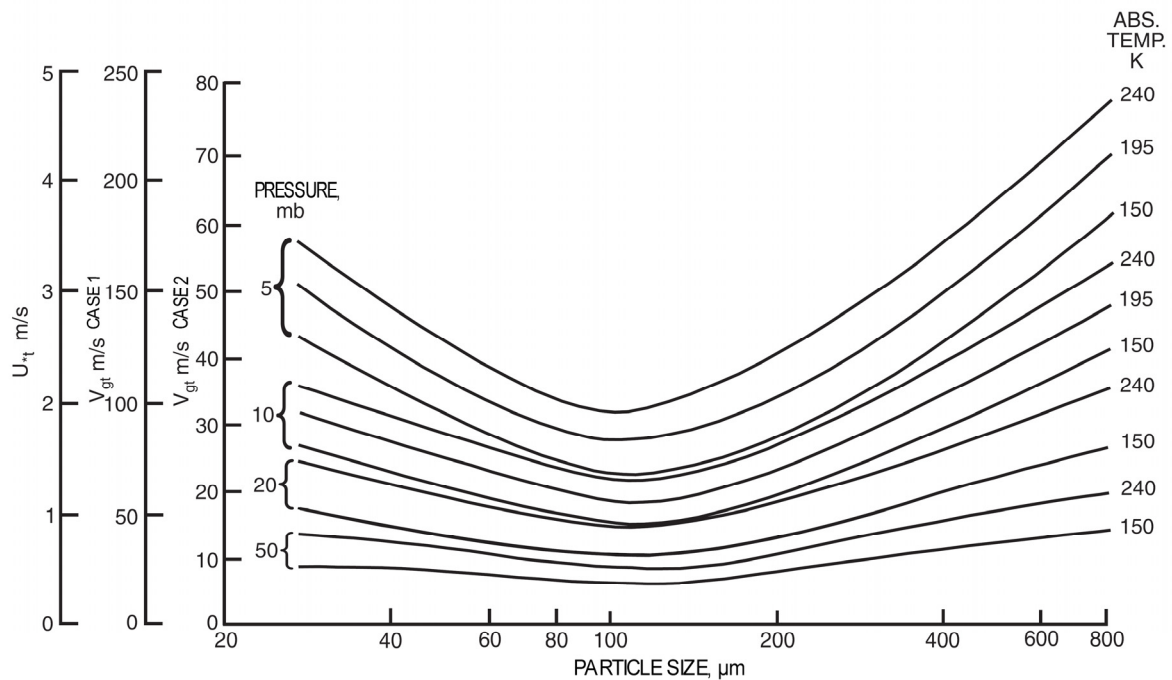

Figure 9: Particle threshold curve as a function of particle size for representative Martian surface pressures and temperatures [*Greeley et al.*, 1980].
Case 1: free stream velocity above boundary layer for winds blowing over a flat surface of erodable grains:
Case 2: surface with cobbles and small boulders.

The transition from saltation to suspension is not a sharp boundary. It depends on a critical value of the grain diameter, which in turn depends on the relationship of terminal velocity (u_f) to threshold friction speed (u_{*t}) [*Parteli and Herrmann*, 2007]. *Iversen et al.* (1976a) placed this transition at the point where the ratio of terminal velocity to threshold friction speed (u_f / u_{*t}) is 1.0. Fig. 10 illustrates these boundaries for Earth and Mars,

respectively. The particle diameters corresponding to this ratio are about 210 μm for Mars and about 52 μm for Earth [*Iversen et al.*, 1976a; *Greeley and Iversen*, 1985; *Edgett and Christensen*, 1991]. In a thinner atmosphere, the greater initial grain velocity coupled with the lower gravity causes the grains' saltation path to lengthen. Thus, the path lengths of grains of up to 210 μm begin to approach infinity [*Edgett*, 2002]. *Edgett and Christensen* (1994) showed that particles ranging from ˜50 μm to ˜210 μm may be subject to short-term suspension at friction velocities.
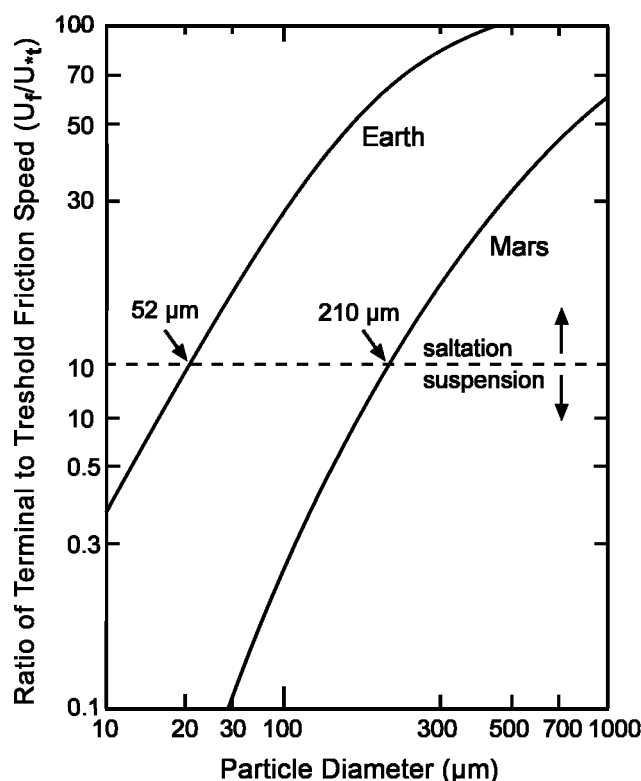
Figure 10: Ratio of terminal speed (u_f) to threshold friction speed (u_{*t}) as a function of particle size for Earth and Mars [*Edgett and Christensen*, 1991].

It is, therefore, clear that because of the higher surface friction velocities needed to move particles at low atmospheric pressures and a lower gravity, larger grains can become suspended on Mars than on Earth. This also suggests that Martian dunes may be significantly coarser-grained than terrestrial ones. *Edgett and Christensen* (1991) suggested – and proved - that the average grain size in Martian dunes is in the medium to coarse range. In comparison, the average grain size of terrestrial dunes is in the fine to medium sand range. Although it takes stronger winds to saltate particles on Mars and the saltating particles are coarser-grained than on Earth, trajectories are longer and flatter, varying with temperature and atmospheric conditions [*White*, 1979; *Iversen and White*, 1982; *Greeley et al.*, 1999; *Fenton et al.*, 2005] Increasing temperatures curtail the height and length of a trajectory path [*White*, 1979]. Average saltation trajectories for Martian particles are about 1 m long and 10 to 20 cm high [*Greeley et al.*, 1992]. *Hartmann* (2003)

specified the trajectory path for particles of 1000 μm grain size and average Martian wind speeds of 5.3 m/s to be up to 1 m high and 3 to 10 m downwind. However, a critical point is that the higher friction velocities needed to move grains call, of course, for correspondingly higher effective wind velocities. Under the present atmospheric conditions of Mars, these wind speeds must be 10 times higher than on Earth [*Greeley et al.*, 1980]. Such wind velocities are very rare on Mars, mostly occurring only during dust storm events [*Sullivan et al.*, 2005]. Wind gusts of a local dust storm on Sol 423, measured by the meteorological sensors of a Viking Lander, reached velocities of 25-30 m/s at 1.6 m above the surface [*Greeley et al.*, 1980; *Moore*, 1985; *Hartmann*, 2003]. *Greeley et al.* (1980) estimated that the wind would have to exceed even these high velocities to cause saltation. In addition, *Ryan and Sharman* (1981) reported that this dust storm caused little or no erosion of the surface materials. So far, substantial erosion and modification of topography was reported only for the dust storm on Sol 1742 measured at the Viking Lander 1 site [*Moore*, 1985]. Thus, researchers suppose that the bulk of the Martian dunes were built up a long time ago when the density of the Martian atmosphere was higher [*Breed et al.*, 1979]. Under present conditions, dune movement is very slow, with most of it probably occurring during dust storms. This is consistent with observations that a proportion of Martian dunes seem to be immobile (at least seasonally) and did not change over several Martian years of observation [e.g. *Breed et al.*, 1979; *Zimbelman*, 2000; *Malin and Edgett*, 2001; *Edgett*, 2002; *Schatz et al.*, 2006; *Tirsch et al.*, 2007]. Observations of moving or disappearing dunes are rare [e.g. *Fenton*, 2005a; *Bourke and Edgett*, 2006; *Bourke et al.*, 2008a]. The reason for this might be that the moving rate is immeasurable, given the limited number of repeated observations spanning several Mars years and the spatial resolutions available. In many studies, comparisons of Viking and MOC images over 4-15 Martian years show no clear evidence of any translation of aeolian dunes across the Martian surface [*Schatz et al.*, 2006]. An analysis of the dark dunes' theoretical inability to move, possibly due to surface consolidation, will be discussed in Sect. 5.5.

3.2 Evidence for Recent Aeolian Transport on Mars

It is a striking fact that although sand is theoretically much more movable than dust (because the cohesion of dust particles hampers movement), transport of windblown particles on Mars is predominantly observed in association with clay-sized particles, i.e. dust storms, dust plumes and dust devils [e.g. *Iversen et al.*, 1976a; *James and Evans*, 1981; *Ryan and Sharman*, 1981; *Moore*, 1985; *Edgett and Malin*, 2000b; *Zimbelman*, 2000; *Cantor et al.*, 2001; *Malin and Edgett*, 2001]. Recent studies from MER landing sites [e.g. *Squyres et al.*, 2003; *Squyres et al.*, 2004; *Arvidson et al.*, 2006; *Squyres et al.*, 2006a; *Squyres et al.*, 2006b] reveal that the dust particles at the surface are aggregated in fragile sand-sized agglomerates which, due to their lower weight, can be much more easily transported than weighty sand-sized particles or cohesive clay-size particles [*Herkenhoff et al.*, 2004; *Sullivan et al.*, 2008a]. These particles can, in turn, be very easily entrained

and disintegrated into dust particles that are suspendable in dust devils and dust storms [*Sullivan et al.*, 2008a; *Sullivan et al.*, 2008b]. Fig. 11 shows a comparison between large dust aggregates and loose cohesionless fine/very fine mafic sand (200-300 µm) that resembles the dark surface material in the El Dorado dune field (see Fig. 69) at MER Spirit's landing site in Gusev Crater [*Sullivan et al.*, 2008a]. Note the ease with which dust aggregates were crushed into ultra-fine unresolved particles by the contact plate imprint of the Mössbauer spectrometer (MIMOS II). The instrument is described in detail by *Klingelhöfer et al.* (2003), *Squyres et al.* (2003), and *Morris et al.* (2006).
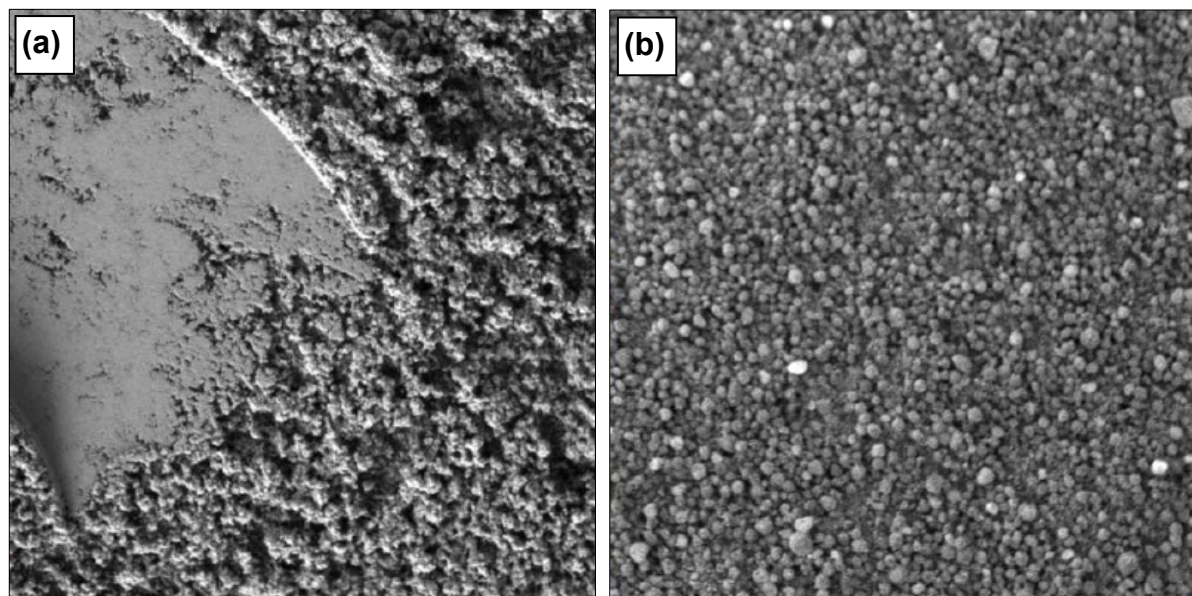
Figure 11: Comparison of aggregated dust particles and loose sand at different sites in Gusev crater **(a)** Large 'popcorn-like' aggregates of airfall dust with an imprint of a Mössbauer contact plate showing that agglomerates are easily crushed into ultra-fine unresolved particles (view of Microscopic Imager (MI) on board the Spirit Rover; image is ˜15 mm across). **(b)** Loose cohesionless fine/very fine dark mafic sand (200-300 µm) that resembles the dark material in the El Dorado dune field (MI view, ˜15 mm across). Images obtained from *Sullivan et al.* (2008a).

Although sand transport is much harder on Mars than on Earth, there is some evidence for recent saltation processes on Mars. For example, after the dust storm in March 2005 [*Cantor et al.*, 2006], accumulations of sand grains were found on the 1 m-high deck of the Mars exploration rover Spirit [*Greeley et al.*, 2006]. Changes in the surface albedo of Gusev Crater (darkening) also resulted from material transport during the dust storm of March 2005. This indicates the removal and redistribution of a brighter fine-grained dust cover as well as coarser grained material on the Gusev Crater floor [*Cantor et al.*, 2006]. The absence of impact craters on dune surfaces and sharp brinks at the top of their slip faces suggests that a certain portion of Martian dunes might have an unaltered morphology [*Edgett and Malin*, 2000b; *Bourke et al.*, 2008a]. Other changes in dune slip faces, such as lineations interpreted as dry grain flows on dune avalanche faces [e.g. *Edgett and Malin*, 2000b; *Reiss and Jaumann*, 2003; *Fenton*, 2006], wind streaks emanating from dunes or dark spots [*Edgett and Malin*, 2000b], and other dark streaks extending

downwind from dunes [*Breed et al.*, 1979] might also indicate local sand transport. Further evidence of current sand movements on Mars comes from slight changes in the orientation and brightness of wind streaks at Victoria Crater revealed by the comparison of MOC and HiRISE images [*Bridges et al.*, 2007]. Evidence of the recent mobilization of fine mafic sand was observed by the rover Spirit close to the 'Home Plate' site at Gusev Crater. Small dark ripples have moved by about 2 cm towards the rover during a wind event lasting five Martian Sols [*Sullivan et al.*, 2008a]

3.3 Sand Sources, Formation Processes, and Bed Forms on Mars and Earth

Pye and Tsoar (1990) name three basic requirements for sand-sea or dune-field formation: (a) a large sand supply, (b) adequate wind energy for material transport, and (c) suitable and persistent climatic and topographic conditions allowing the accumulation of large and thick sand masses. On Earth, deserts are often located in basins and in the vicinity of huge river systems [*Besler*, 1992]. Again on Earth, aeolian transported sands and desert regions can generally be found near rivers, especially at the termination of huge (mostly endorheic) drainage basins, i.e. upon or at the margin of vast alluvial fans. The Sahara, the Rub' al Khali in Arabia, the Simpson desert in Australia, and parts of the Namib erg are examples of that similarity of location on Earth [*Besler*, 1992]. In the case of exorheic rivers, the accumulated fluvial sands are deflated out of the estuary regions at low water and transported to the desert regions nearby. Further sand sources on Earth are beaches and coasts, where large amounts of sand are produced by general shoreline erosion processes like abrasion or corrosion. In addition, loess generated by glaciers as well as the disintegration and weathering of solid rock (primarily sandstone) can produce huge amounts of sandy material [*Cooke and Warren*, 1973; *Besler*, 1992; *Cooke et al.*, 1993]. *Greeley and Iversen* (1985) classify the processes of particle formation on terrestrial planets as weathering (physical and chemical), cataclastic processes (disintegration of particles caused by collision during fluvial or aeolian transport, fragmentation caused by impact cratering, and crushing and grinding due to mass movements), volcanism, biochemical precipitation and biological activity (e.g. mechanical breaking by tree roots), and aggregation (building of sand-sized particles from aggregates of smaller particles).

Except for the biological processes, the mechanisms of sand formation on Mars are similar to those on Earth, albeit with a different emphasis. Due to the lack of active river systems and shorelines, volcanic activity might be the main sand-producing process on Mars today, resulting in large amounts of fine particles generated from pyroclastic deposits such as ashes and scoria [*Greeley and Iversen*, 1985; *Baratoux et al.*, 2007]. Aeolian erosional processes such as corrasion or abrasion, and deflation (see Sect. 2.1.3), which erode the harder volcanic basalts and remove small particles, are remarkable land-forming processes on Mars, producing some aeolian sediments over long periods. In former times, when liquid water was present on the Martian surface, i.e. between the late Noachian and

the late Amazonian period, the huge valley networks and outflow channels on Mars probably generated enormous amounts of sediment by fluvial processes. Glaciers on Mars may similarly have produced enormous amounts of sediment, although not as efficiently. Another important particle-producing process on Mars is fragmentation caused by impact shock waves [*Baratoux et al.*, 2007].

Breed et al. (1979) classified sand sources as either primary (disintegration of bedrock) or secondary (fluvial, marine, and glacial sediments). They suppose that the products of impacts, volcanism, and former fluvial activity provided a major part of the secondary sources on Mars. However, the supply of solid particles to form dune sands is sparse on Mars in comparison to Earth [*Breed et al.*, 1979]. A rising number of authors [e.g. *Greeley*, 1979; *Herkenhoff et al.*, 2004; *Landis et al.*, 2004; *Herkenhoff et al.*, 2006; *Sullivan et al.*, 2008a] suggest that dust particles aggregated by electrostatic forces might represent a notable amount of dune-forming particles capable of saltation on Mars.

The type of material accumulation depends on the sand supply, the wind regime (strength and direction), the local topography, and the distance from the source [*Breed et al.*, 1979; *McKee*, 1979]. The smaller the sand supply, the smaller the potential for bed forms to develop and sand sheets to accumulate. Dunes are more likely to develop if more material is available and the wind regime is favourable [e.g. *Bagnold*, 1954; *Pye and Tsoar*, 1990; *Wiggs*, 2002]. The most famous dune classification scheme was developed by *McKee*, (1979) and adopted by many workers. *McKee* (1979) classified dunes based on two descriptive attributes, namely the shape of the sand body and the number and position of slip faces, arriving at three major dune categories: basic or simple dunes, compound dunes, and complex dunes. An overview of dune types is given in Fig. 12; the most common types will be discussed below.

Simple dunes are spatially separated individual dunes [*Pye and Tsoar*, 1990]. A frequent form is the crescent-shaped barchan dune, which develops under conditions of limited sand supply and unidirectional winds. As the amount of sand increases, barchanoid ridges (parallel rows of coalesced barchans) and transverse dunes (parallel straight ridges) may form under the same wind conditions in gradational sequence [*McKee*, 1979]. These three one-slip face dune types are referred to as 'crescentic' dunes by *McKee et al.* (1979). *Wiggs* (2002) and *Breed et al. (*1979) classify these types as 'transverse' dunes because they are bed forms deposited by wind that generally blows transversely to their main axes. Bimodal wind regimes result in the growth of linear or seif dunes with two slip faces on both sides. Linear dunes, sometimes also referred to as longitudinal dunes, have a simple longitudinal pattern, whereas seif dunes are a sub-type characterised by a meandering shape caused by the bidirectional wind [*Tsoar*, 2008]. Seif dunes may also develop from barchan dunes that are modified by a bi-directional wind regime so that the dune becomes asymmetrical and extends a seif-shaped limb [*Tsoar*, 1984; *Bourke*, 2008]. Star dunes, characterised by multiple slip faces at several radially extending arms and a pyramid-like shape, develop under a complex multi-directional wind regime [*McKee*, 1979; *Schatz et al.*, 2006]. Two winds of equal strength blowing from nearly opposite directions produce reversing dunes. This dune type resembles

transverse ridges but has a second slip face caused by the second wind direction [*McKee*, 1979]. All these simple dune types are prevalent on both Earth and Mars. Crescentic and especially barchan dunes are the most common types on Mars and account for about half the dunes observed on Earth [*Breed et al.*, 1979]. Linear dunes are another type frequently found on Earth [*Tsoar*, 2008], which is however very rare on Mars (see Sect. 5.1). Compound dunes consist of several dunes of the same type, which have coalesced or are superimposed onto each other. Complex dunes consist of two or more dunes of different basic types, which have coalesced or grown together by migrating at different rates [*Breed et al.*, 1979; *McKee*, 1979; *Pye and Tsoar*, 1990]. Multiple combinations of this dune type are common in most sand seas on Earth, such as the desert of Peru [*Grolier et al.*, 1974, cit. in *Breed et al.*, 1979] or the Kelso dunes in southern New Mexico [*Sharp*, 1966, cit. in *Schatz et al.*, 2006]. On Mars, such vast compound and complex dune fields can primarily be found in huge craters in Noachis Terra (formerly named the Hellespontus region), e.g. Proctor, Kaiser, Russell, and Rabe (see Fig. 2 and Appendix). *Breed* (1977) found the dunes in the Kara Kum desert in Turkmenistan and in the Badan Jiling sand sea of the Ala Shan (Gobi) desert in China to be the closest terrestrial analogues in shape and aerial extent.

As an aeolian bed form, the dune is the most impressive deposition type of aeolian sands although the material may also accumulate in sand sheets. *McKee* (1979) describes sand sheets as sand bodies with a flat surface and without slip faces. Sand seas, often referred to as 'ergs' on Earth, consist of both dunes and sand sheets [e.g. *Cooke and Warren*, 1973; *Pye and Tsoar*, 1990; *Cooke et al.*, 1993; *Thomas*, 2000]. A huge sand sea on Mars comprising dunes and sand sheets called the north polar erg can be found around the north polar cap.

The majority of the terrestrial dune types shown in Fig. 12 can be found on Mars, so that they may be used as analogues in Martian studies. However, some dune types develop under conditions for which Mars is not suitable. For example, Mars exhibits no parabolic dunes such as can be found in several terrestrial deserts (e.g. in the western USA: White Sands, Alkali Lake, Mosses lake, Juniper Flats) [*Zimbelman and Williams*, 2007]. One factor determining the formation of parabolic dunes is the stabilization of the sand mass by vegetation, which is not present on Mars.

All previously discussed dune types are made of dark material on Mars. There is a further very common aeolian bed form on Mars that is not made of dark material. The so-called 'transverse aeolian ridges' (TARs) are light-toned linear bed forms that often cover the floors of troughs and typically follow their course [e.g. *Malin and Edgett*, 2001; *Bourke et al.*, 2003; *Balme and Bourke*, 2005; *Balme et al.*, 2008; *Berman et al.*, 2008]. In many places, it is obvious that dark dunes overlie the TARs, indicating that the dark bed forms are much younger than the bright linear features [*Berman et al.*, 2008].

The dark dunes on Mars are relatively young and were recently active or are active today, as indicated by the absence of impact craters on the dune surfaces where even high-resolution HiRISE data (see Sect. 4.6) could not reveal any small craters. Therefore, dark dunes cannot be dated by the crater size-frequency method described in Sect. 2.1.2. However, small impact craters were found, for example, at the top of smaller bright

transversal dunes (TARs) at Nirgal Vallis [*Reiss*, 2006], proving the inactivity of these bright aeolian bed forms under current climatic conditions.
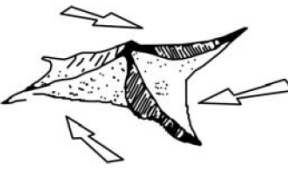
Dune Type		Number of slip faces	Major control on form	Formative wind regime	Nature of movement
Zibar		0	Coarse sand	Various	Limited
Dome dune		0	‖	‖	‖
Blow out		0	Disrupted vegetation cover	‖	May extend down wind
Parabolic dune		1	‖	Transverse, Unimodal	Slow, nose migration
TRANSVERSE DUNES					
Barchan dune		1	Wind regime and sand supply	‖	Forward migration
Barchanoid ridge		1	‖	‖	‖
Transverse ridge		1	‖	More directional variability than for barchains	‖
LINEAR DUNES					
Linear ridge		1 - 2	‖	Bimodal / wide unimodal	Extending
Seif dune		2	‖	Bimodal	‖
Reversing dune		2	‖	Opposing bimodal	May migrate if one mode dominant
Star dune		3+	‖	Complex, Multimodal	Vertical arrection

Figure 12: Classification of major dune types (adapted from *Wiggs* (2002)).

3.4 Areas of Dark Material Distribution

The dark areas on the face of the planet (Fig. 1) suggest at first glance that this material is nearly globally distributed. A closer look reveals that this particulate material is frequently associated with impact craters (especially in the southern hemisphere) and other depressions (such as Valles Marineris), the north polar region, large impact basins (Hellas and Argyre), and the vicinity of volcanic outcrops (such as Cerberus and Syrtis Major) [e.g. *Breed et al.*, 1979; *Poulet et al.*, 2003; *Fenton*, 2005b; *Langevin et al.*, 2005; *Baratoux et al.*, 2007; *Grégoire et al.*, 2007].

A statistical analysis of the geographical distribution of dark dunes was done by *Mullins et al.* (2005) within the framework of the Mars Global Digital Dune Database (MDG[3], see Sect. 4.7.2). They report that 92 % of a total of 626 dune field deposits identified between +/-65 degrees latitude are located in the southern hemisphere. About 76 % or 475 dune fields are located within impact craters. Most of the intra-crater dune fields (413) are also situated in the southern hemisphere, which is to be expected, given the distribution of craters on Mars and the higher erosion rates in the northern hemisphere [*Armstrong and Leovy*, 2005]. The northern hemisphere only contains 42 intra-crater dune fields. The cumulative area identified as covered with dark dune fields between +/- 65° N/S is 60,068 km[2] [*Mullins et al.*, 2005]. Fig. 13 provides an overview of dark dune sites on Mars as recorded in the MDC[3]. There are many more localities covered with dark material on Mars, especially in the polar regions. However, the figure quoted above gives a general impression of the distribution of dark dunes on Mars.
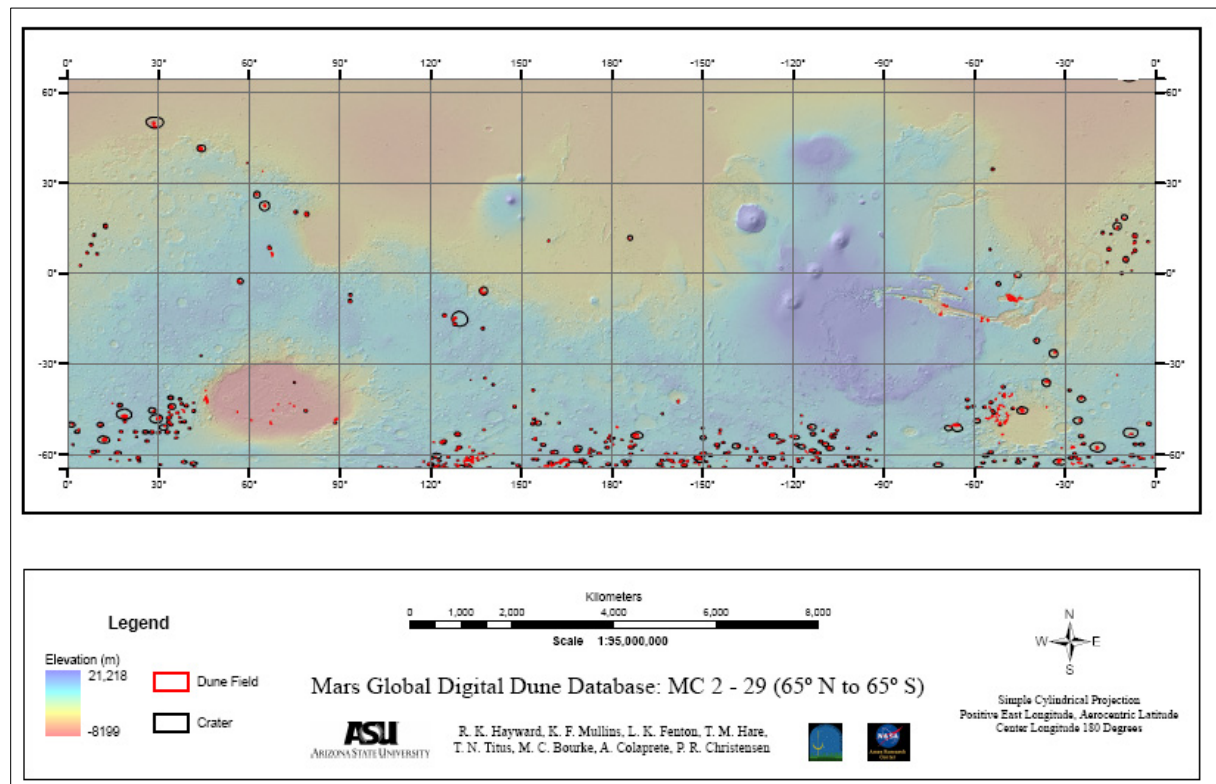

Figure 13: Distribution of dark dunes on Mars as catalogued in the MCD[3] [*Hayward et al.*, 2007b].

As Fig. 13 shows, most of the dunes on Mars are found on crater floors [*Greeley et al.*, 1992; *Fenton et al.*, 2007]. The craters are thought to act as sediment traps for aeolian materials [*Jaumann et al.*, 2006]. The wind blowing over a crater rim leaves particles on the crater floor, often near the downwind crater wall [*Hartmann*, 2003]. Dark material particles may also be deposited downwind outside the crater, where they form wind streaks (i.e. dark depositional wind streaks, Type II streaks[1] according to *Thomas et al.*, (1981)). The most prominent site for huge dune fields on the floors of large Martian impact craters is the Noachis Terra region [*Breed*, 1977; *Fenton*, 2005b]. Dunes in the southern hemisphere upward of 50° S were recently mapped and classified by *Fenton and Hayward* (2008). Preliminary results show that most of the dunes are located in impact craters, whereas the highest densities were logged in the area between 60° S and 80° S. Dune classification showed progressive dune degradation towards the South Pole, which is likely indicative of a climate change postdating the dune formation [*Fenton and Hayward*, 2008].

Furthermore, dark dune fields or ergs are known from some few sites outside of craters or other distinct geographical features, e.g. in the eastern Thaumasia region [*Silvestro et al.*, 2008] and in Aonia Terra [*Silvestro and Ori*, 2008]. Although located in the large flat plain of Gusev Crater, the dark dune field called 'El Dorado' close to the landing site of MER Spirit [*Sullivan et al.*, 2008a] cannot be directly associated with a typical impact crater floor site.

Most north polar dunes are found at Chasma Boreale and Olympia Undae; they have been studied by many authors [e.g. *Tsoar et al.*, 1979a; *Tsoar et al.*, 1979b; *Thomas and Gierasch*, 1995; *Herkenhoff and Vasavada*, 1999; *Edgett et al.*, 2003; *Bourke et al.*, 2004; *Tanaka and Hayward*, 2008]. The source of the Chasma Boreale materials is supposed to be a suite of sand-rich layers exposed in the scarps of the chasm [*Schatz et al.*, 2006]. *Tanaka et al.* (2008) reported that the north polar erg dunes have a particular local source in the Planum Boreum cavi unit. Although these dark polar materials have a similarly low albedo and generate bed forms similar to those of the dark materials in lower latitudes, they exhibit a remarkable difference in thermal behaviour. Their thermal inertia values range around 75 $Jm^{-2}K^{-1}s^{-1/2}$ (cf. Sect. 5.5.3), indicating much finer material [*Paige et al.*, 1994; *Vasavada et al.*, 2000; *Putzig et al.*, 2008]. *Herkenhoff and Vasavada*, (1999) believe that aggregation of low-density particles is the reason for these low thermal inertia values (cf. Sect. 3.2). A further difference between the north polar dunes and those in lower latitudes lies in their mineralogical composition, which is dominated by

---

[1] *Thomas et al.* (1981) classified wind streaks on Mars according to albedo contrast and point of origin (topographic obstacles or sediment deposits) as follows:

Type I (b): modification of wind flow by a topographic obstacle → bright depositional streaks

Type I (b): modification of wind flow by a topographic obstacle → dark erosional streaks

Type I (m): modification of wind flow by a topographic obstacle → mixed-tone streaks

Type II: streaks associated with a source deposit, deflation of a deposit of wind transportable material → dark tongues emanating from dark splotches inside depressions

sulphates (such as gypsum) rather than basaltic materials [*Langevin et al.*, 2005; *Fishbaugh et al.*, 2007], indicating them as secondary weathering products.

Other deposits of dark material can be found along the walls of Valles Marineris, in the Coprates and Juventae chasmata [*Geissler et al.*, 1990b], in Candor Chasma [*Lucchitta*, 2001], and in the Melas and Ganges chasmata [*Baratoux et al.*, 2007] where they form dunes and dark mantles. The dark material in Valles Marineris is of a mafic composition [*Geissler et al.*, 1990b] similar to the dark dune material inside the craters. *Lucchitta* (1990) supposes that a portion of this dark material was derived from local dark outcrops in knobs or from dark layers in interior deposits or trough walls (cf. Sect. 5.2). Alternatively, part of this material may be derived from relatively young pyroclastics from local sources reworked by the wind [*Lucchitta*, 2001].

Dark dune fields in volcanic regions were reported for Syrtis Major (Nili Patera dune field) [e.g. *Bishop*, 1999; *Poulet et al.*, 2003; *Hiesinger and Head*, 2004] and for the Cerberus Region [*Grégoire et al.*, 2007]. Several studies have been concerned with the Nili Patera dune field. *Poulet et al.* (2003) analyzed the mineralogical composition of these dunes, finding that their constituent elements resemble the bulk of dark dune material in craters, i.e. pyroxenes and olivines. Bishop (1999) supposed that these dunes were recently active because of the lack of superimposed features or indications of degradation as well as the morphology of the dune crest lines. The Nili Patera dune field is incorporated in the analysis of the present study.